Photon statistics of a superradiant laser based on cold atoms of Strontium-88

Neven Gentil

supervised by

Stefan A.Schäffer

August 2023 - June 2024

Summary:

- What is superradiance? How do we achieve this state of lasing?
- The superradiant experiment: atoms of strontium and the multilevel structure
- The first order correlation function g^1: what does this physically mean?
- Standard setup for g^1 and its limitations
- The balanced heterodyne setup
- Electronic noise reduction
- Verifications
- g^1 for a standard laser
- g^1 for the superradiant laser
- Numerical simulation as a comparison
- Conclusion.

Introduction

Experiment

Results

What is superradiance? How do we achieve this state of lasing?

Cavity: two partially reflective mirrors. One mode of the cavity must fit the gain medium frequency: they must be in “resonance”

Composition of a laser: cavity + gain medium

By constructive/destructive interference, the cavity field is restricted to well defined frequencies (called “modes”)

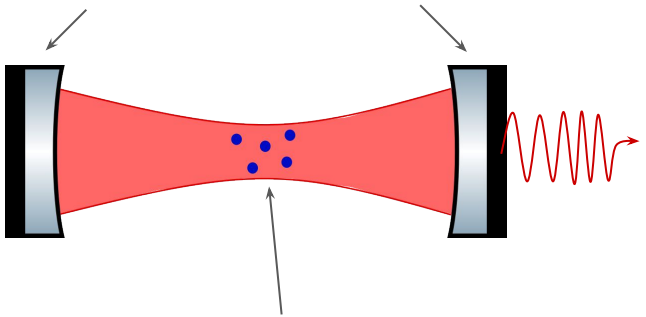

Gain medium: any “two-level” system

Excited state

“Rest” state

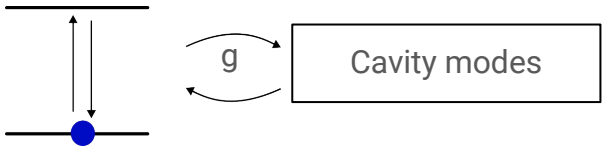

g: coefficient describing the strength of interaction between the gain medium and the cavity field/modes

Two possibilities:

- $g \gg \kappa$: strong coupling
- $g \ll \kappa$: weak coupling

The cavity loss rate (κ) is linked to the reflectivity of the mirrors (coefficient “r”)

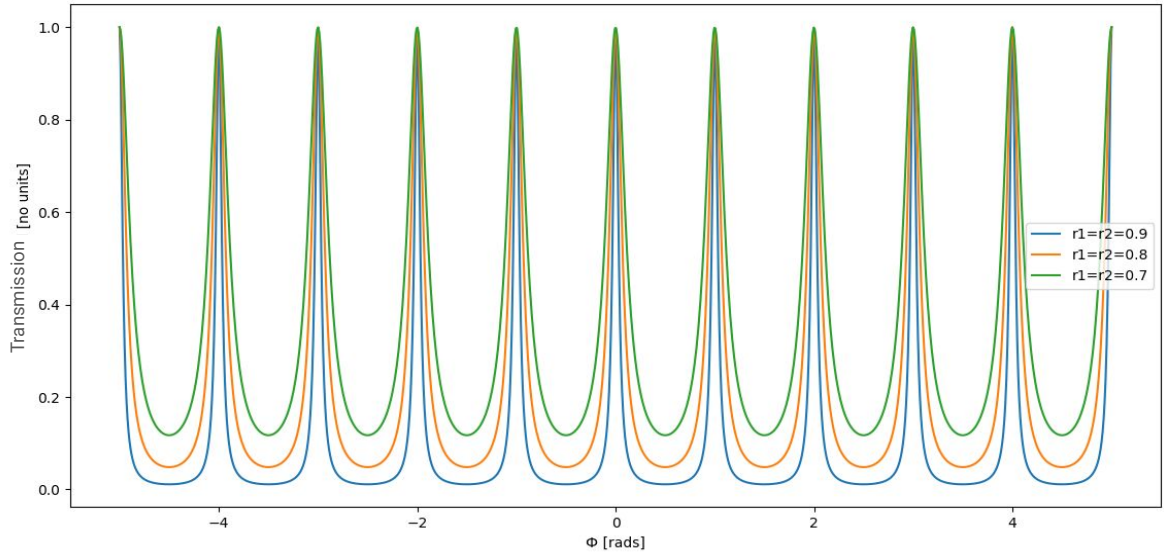

High reflectivity: narrow linewidth allowed for the cavity modes = narrow cavity linewidth
Low reflectivity: broad linewidth allowed for the cavity modes = broad cavity linewidth

“Standard” laser = good cavity regime ⟹ the gain linewidth is broader than the cavity linewidth

This is achieved by **high reflectivity** of the mirrors: the photons inside the cavity make many round-trip before exiting.

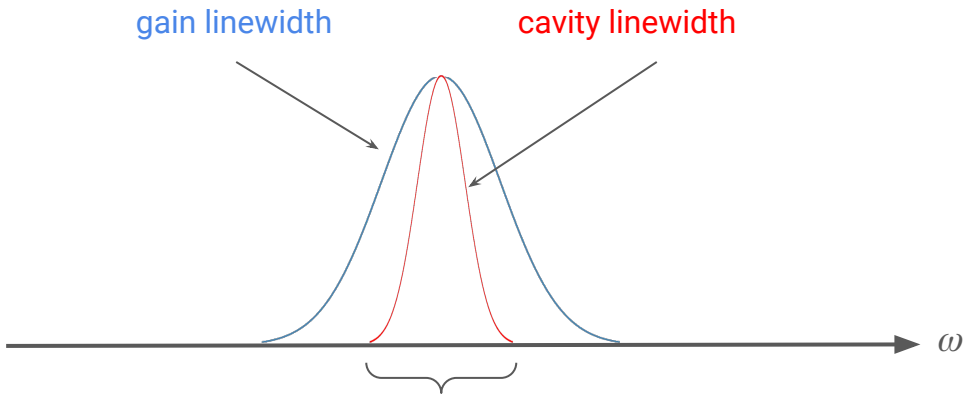

The output frequency spectrum is restricted to the narrower linewidth: here the cavity linewidth.

The cavity linewidth is influenced by mechanical fluctuations ⟹ the spectrum linewidth is influenced by mechanical fluctuations

“Superradiant” laser = bad cavity regime ⟹ the gain linewidth is narrower than the cavity linewidth

This is achieved by **low reflectivity** of the mirrors: the photons quickly exit the cavity

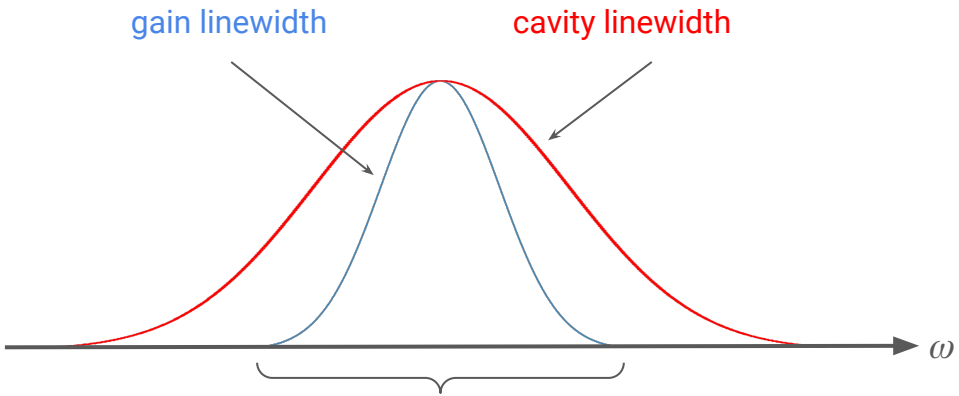

The output frequency spectrum is restricted to the gain linewidth.

Thanks to the few round-trip, the gain linewidth is almost not influenced by mechanical fluctuations ⟹ the frequency spectrum is mainly determined by the two-level transition spectrum of the gain medium.

Superradiance:

- Bad-cavity regime
- Strong-collective coupling

Coherence time/length determined by the gain medium, here cold atoms of Strontium-88. In theory, the output linewidth may be as narrow as the transition linewidth used.

The cavity is weakly coupled to one single atom ($g \ll \kappa$) but **strongly coupled to the ensemble** ($Ng \gg \kappa$ with N the number of atoms)

The superradiant experiment: atoms of strontium and the multilevel structure

Why ^{88}Sr?

- **The most abundant isotope of strontium** at ~82% by mass.
- No nuclear spin: **simpler level structure compared to other isotopes** and makes it easier to work with, especially for the many transitions involved in the repumping/cooling scheme.
- Two electrons in their outermost shell: structure of **electronic transitions that is particularly useful in quantum metrology**.
- The transition $^1S_0$ -$^3P_1$ has a **linewidth of 7.5 kHz.**

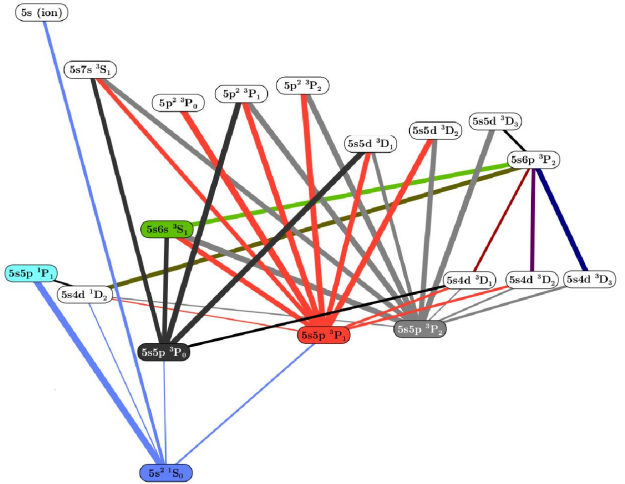

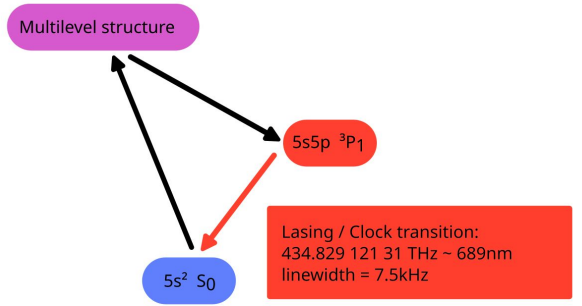

The first order correlation function g¹: what does this physically mean?

Non-stationary case

$$g^1(t_1,t_2) \overset{\text{def}}{=} \frac{\langle E^*(t_1)E(t_2)\rangle}{\sqrt{\left\langle |E(t_1)|^2\right\rangle \left\langle |E(t_2)|^2\right\rangle}}$$

$$t_1 - t_2 \overset{\text{def}}{=} \tau$$

Stationary case

$$g^1(\tau) = \frac{\langle E^*(\tau)E(0)\rangle}{\left\langle |E|^2\right\rangle}$$

Frontier of the quantum world

$$\hat{E}^+ = i\sum_{\vec{k},\lambda}\sqrt{\frac{\hbar\omega_k}{2\epsilon_0 V}}\hat{a}_{\vec{k},\lambda}e^{i\vec{k}.\vec{r}}\vec{e}_{\vec{k},\lambda} \qquad \hat{E}^- = -i\sum_{\vec{k},\lambda}\sqrt{\frac{\hbar\omega_k}{2\epsilon_0 V}}\hat{a}^\dagger_{\vec{k},\lambda}e^{-i\vec{k}.\vec{r}}\vec{e}^*_{\vec{k},\lambda}$$

"You shall not pass!"

Non-stationary case

$$g^1(t_1,t_2) = \frac{\langle \hat{a}^\dagger(t_1)\hat{a}(t_2)\rangle}{\sqrt{\langle \hat{a}^\dagger(t_1)\hat{a}(t_1)\rangle \langle \hat{a}^\dagger(t_2)\hat{a}(t_2)\rangle}}$$

$$t_1 - t_2 \overset{\text{def}}{=} \tau$$

Stationary case

$$g^1(\tau) = \frac{\left\langle \hat{a}^\dagger(\tau)\hat{a}(0)\right)\right\rangle}{\langle \hat{n}\rangle}$$

Perfectly coherent signal (perfectly well defined phase and frequency)

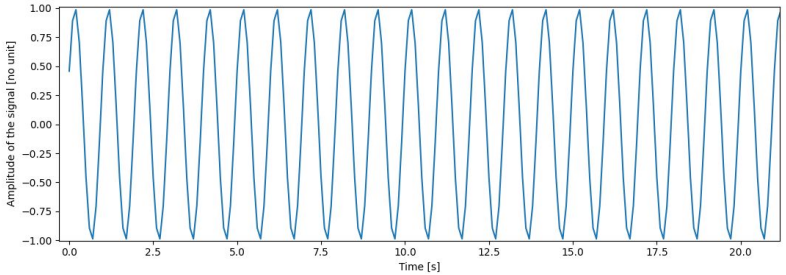

Chaotic signal generated by collision broadening (random phase jumps)

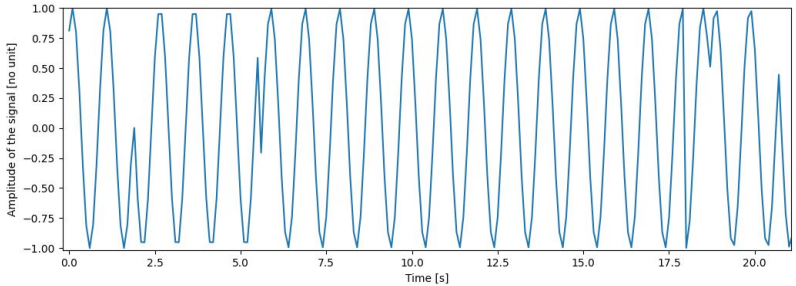

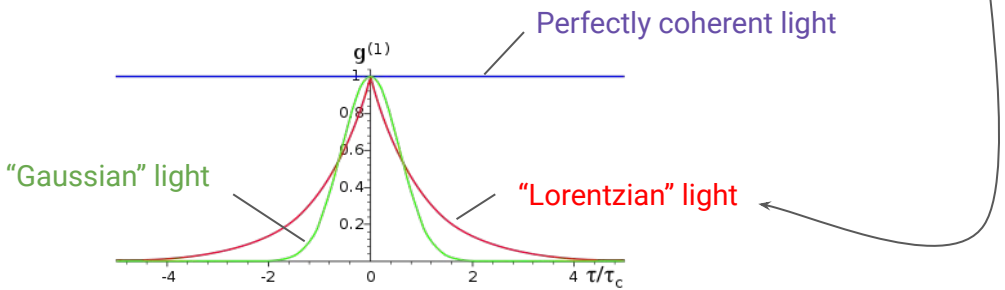

The first order correlation function g¹: what does this physically mean? - 10

Standard setup for g^1 and its limitations

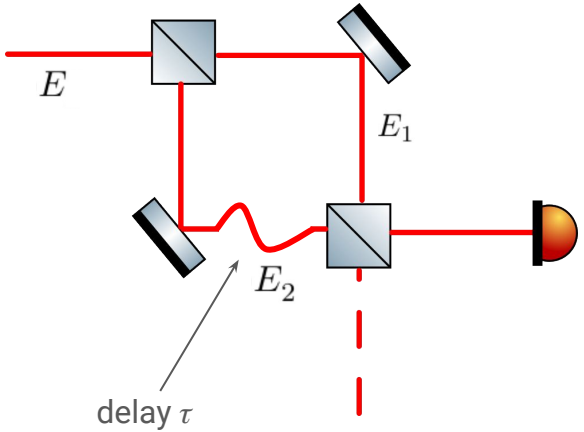

$$I_{detected}(\tau) = I_1 + I_2 + 2\sqrt{I_1 I_2}\Re\{\gamma_{1,2}(\tau)\} \qquad \gamma_{1,2}(\tau) \stackrel{\text{def}}{=} \frac{\langle E_1(t)E_2^*(t+\tau)\rangle_T}{\sqrt{\langle I_1(t)\rangle_T \langle I_2(t+\tau)\rangle_T}} \in \mathbb{C}$$

$$I_{detected,max} = I_1 + I_2 + 2\sqrt{I_1 I_2}|\gamma_{1,2}|$$

$$I_{detected,min} = I_1 + I_2 - 2\sqrt{I_1 I_2}|\gamma_{1,2}|$$

$$\nu \stackrel{\text{def}}{=} \frac{I_{max} - I_{min}}{I_{max} + I_{min}} \longrightarrow \nu = \frac{I_{detected,max} - I_{detected,min}}{I_{detected,max} + I_{detected,min}} = \frac{2\sqrt{I_1 I_2}|\gamma_{1,2}|}{I_1 + I_2}$$

Limitations:

- The detector must follow a frequency in order of **THz**
- The detector must detect the given intensity from the cavity (**as low as it can be**)
- **Highly sensitive to noise** (i.e dust)

The balanced heterodyne setup

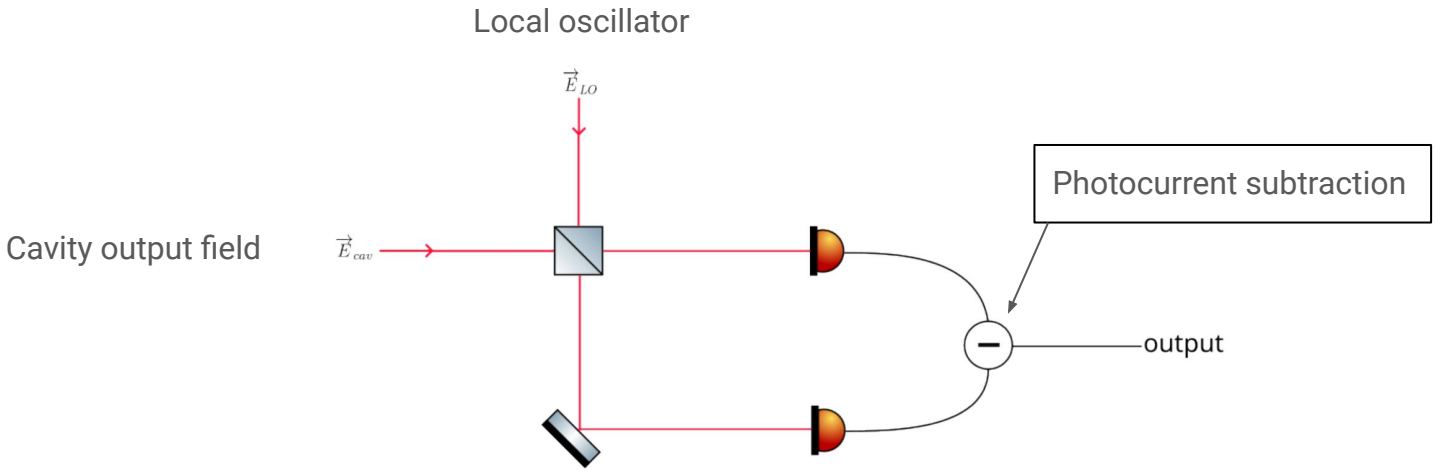

Advantages:

- Remove correlated noise (i.e happening in both arms)
- Detected power tuned by the local oscillator
- The component detected is the frequency difference of the LO and the cavity field: about 43MHz in that case

Electronic noise reduction

Objective: change an electrical component in order to move THIS hollow to THIS position (~43MHz)

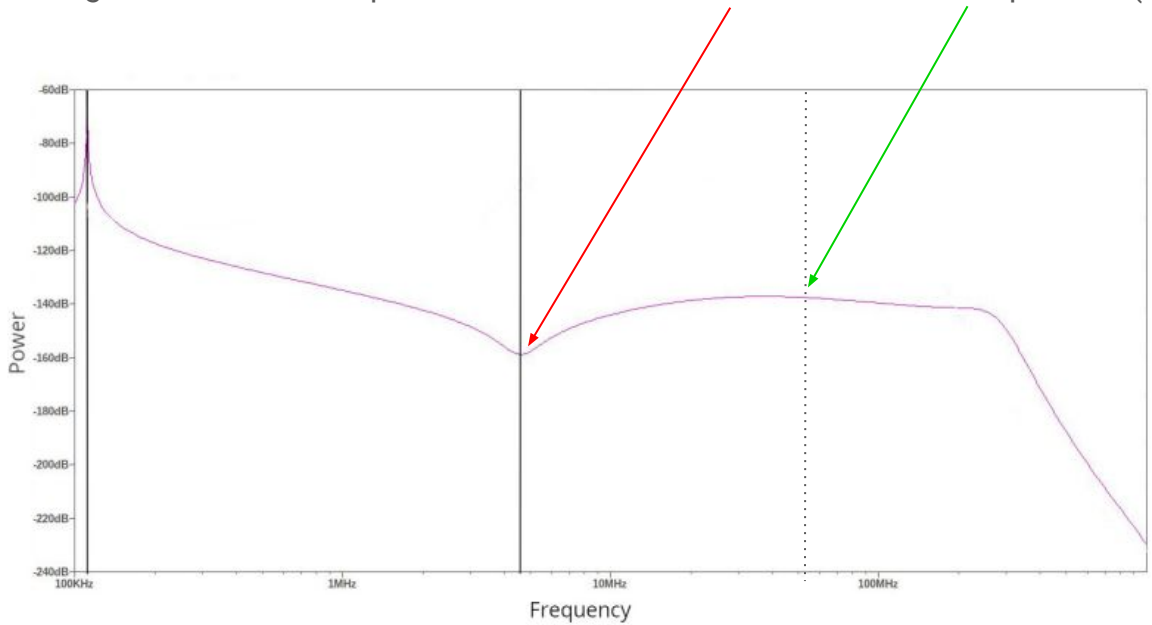

Simulated **noise gain graph** with the original components. The notch filter is localised by the left vertical line. The tank filter is localised on the right.

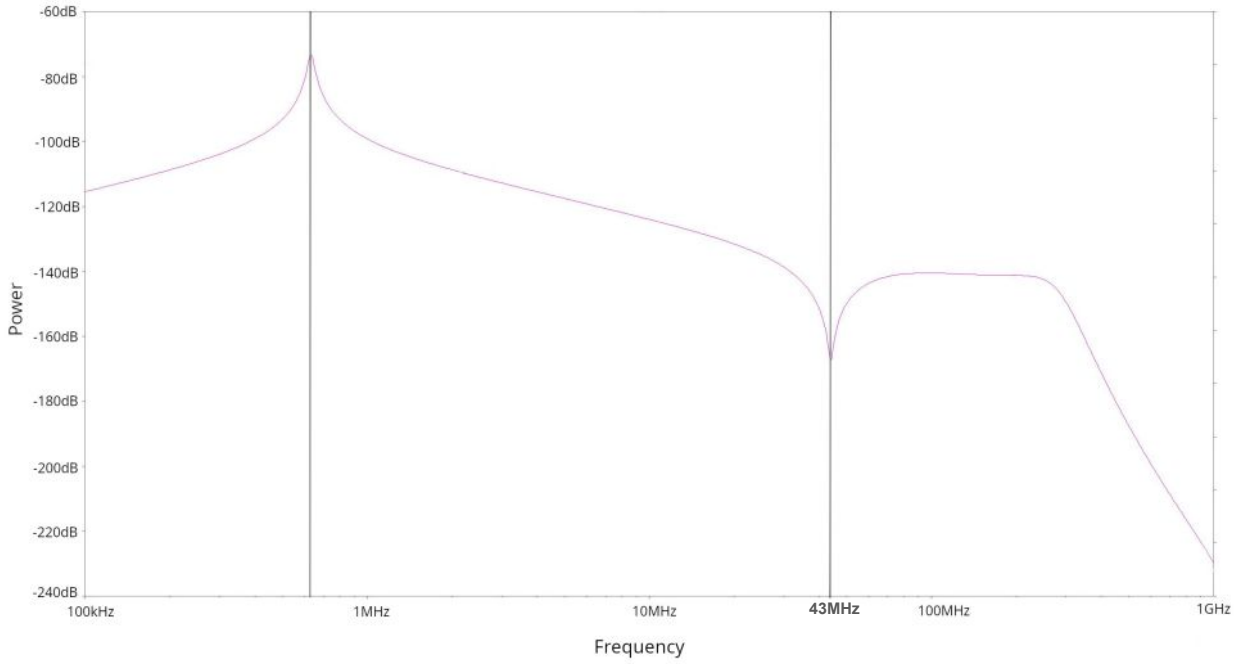

Simulated noise gain graph with the new component (inductor)

Verifications

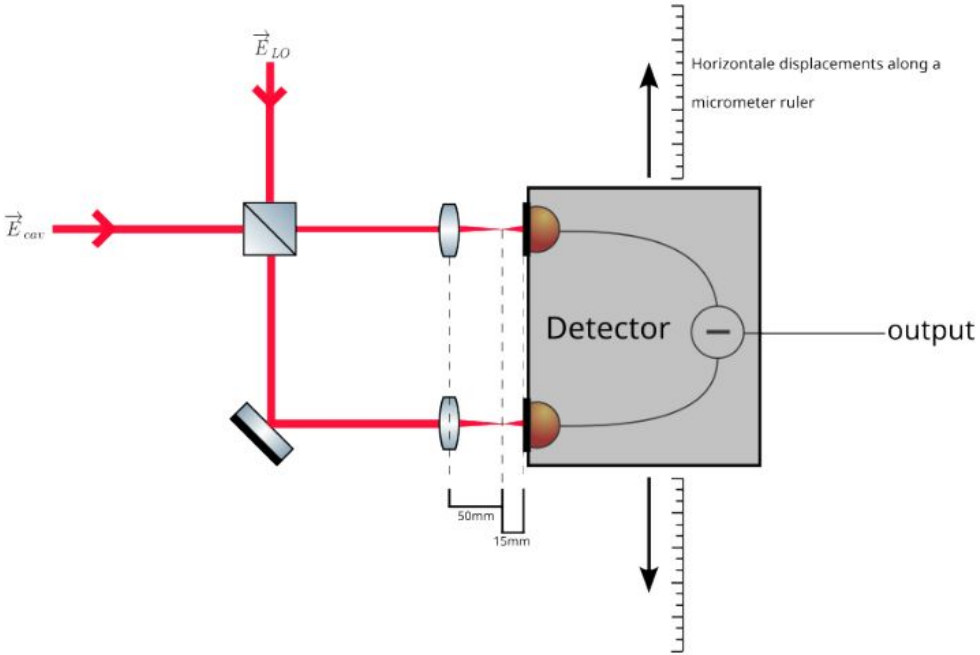

Heterodyne experiment with lens added. The detector moves along a micrometer ruler in order to tune precisely the relative position between the photodiodes and the beams.

Diode/beam relative size

- The laser beam size is smaller than the photodiodes. The voltage output increases, reach a plateau of constant voltage output, then decreases.

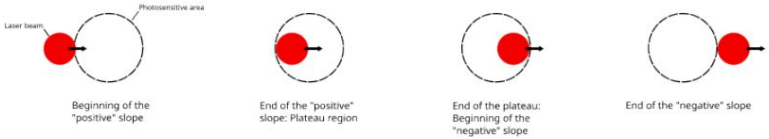

- The laser beam size is equivalent to the photodiodes. The voltage output increases, reach a maximal peak of voltage, then decreases.

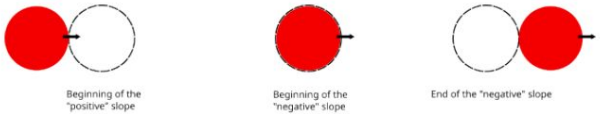

- The laser beam size is bigger than the photodiodes. The voltage output increases, reach a plateau of constant voltage output, then decreases.

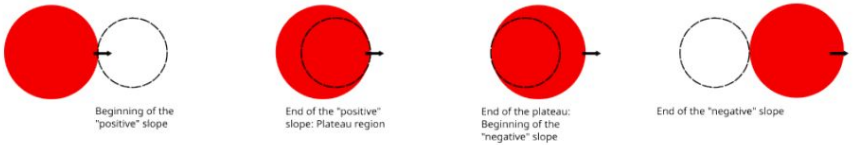

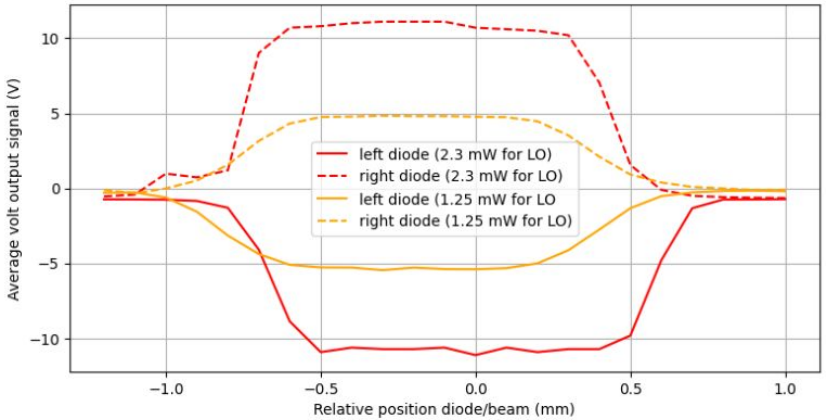

Figure 3.18: Average voltage output of the detector according to the relative position of one of the diode (The other diode is blocked from light), for two different power of the local oscillator. Red curves: each diode receives 1.15 mW of light power. Yellow curves: each diode receives 625 µW of light power.

Power to noise ratio

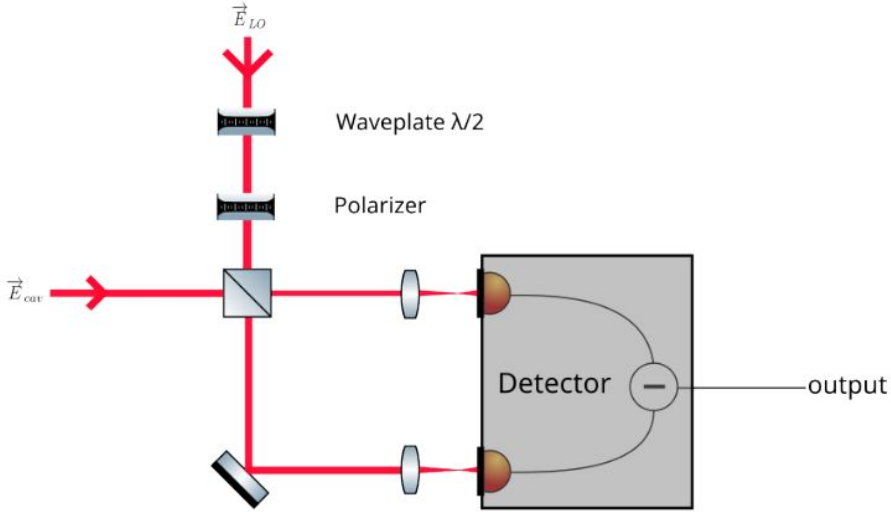

Figure 3.20: Complete setup with the group waveplate+polarizer added before the beam splitter (from the local oscillator's side).

$$\text{Noise power (in watts)} \propto \text{Light intensity (in watts)}$$

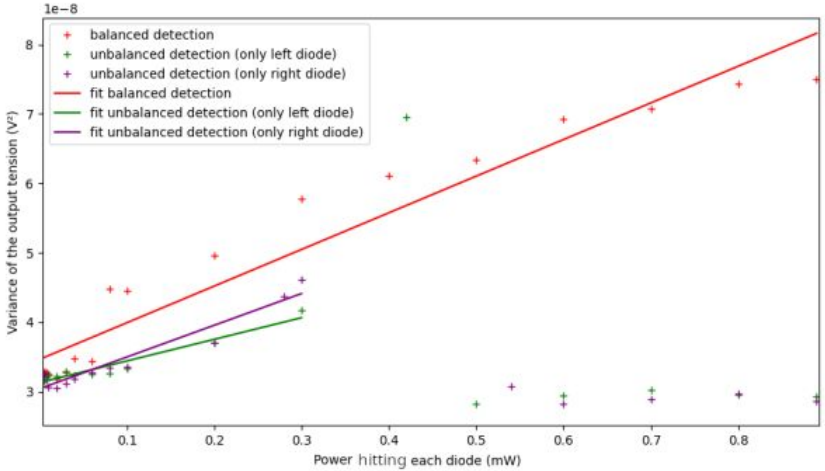

Figure 3.23: Power to noise ratio plot for three different configurations. Cross symbols are experimental data whereas solid straight lines are the associated fit. The red color stands for the balanced detection. The green color and purple color stand for the unbalanced detections: only the left/right diode receives light respectively.

g^{1} for a standard laser

Example of a collected signal (after a numerical band-pass filter applied)

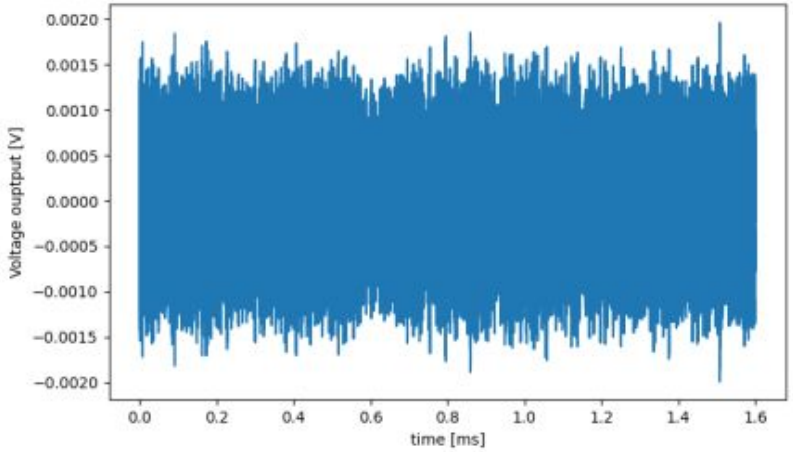

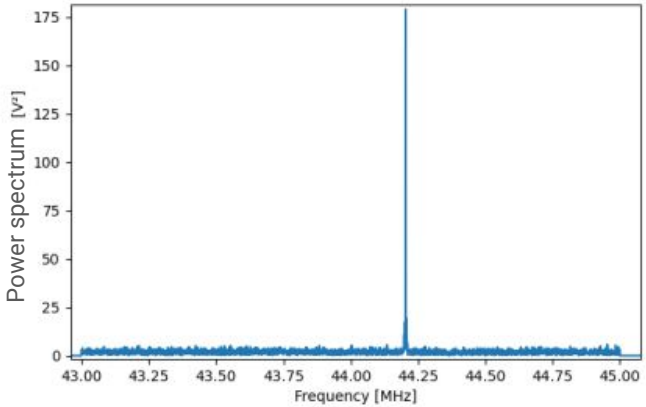

Post-process data analysis

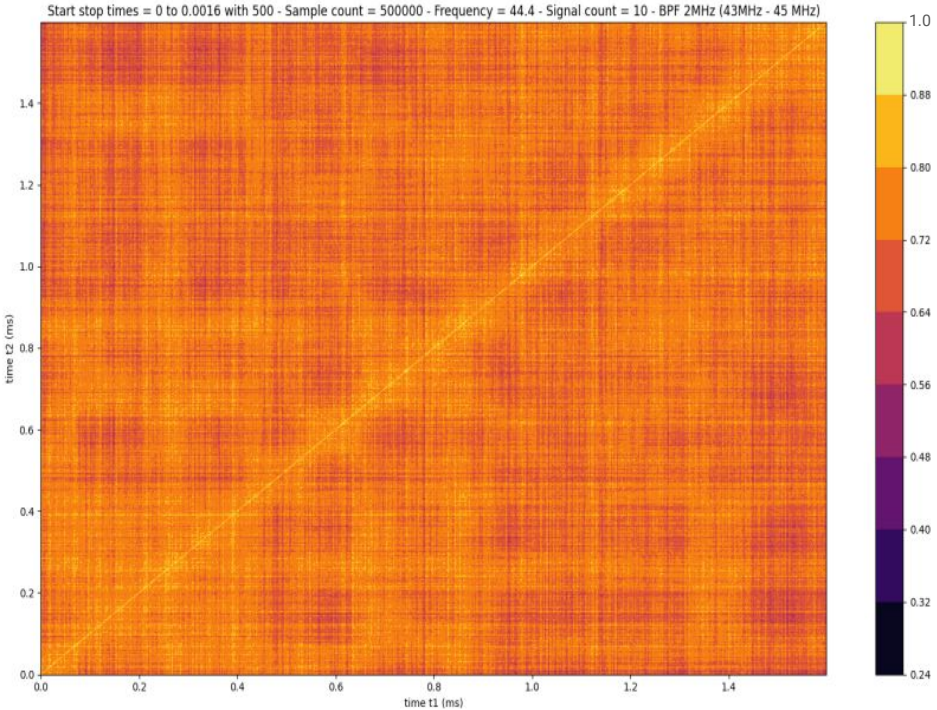

Figure 4.3: Non-stationary plot of $|g^1(t_1, t_2)|$ for a standard laser. Time in milliseconds on both axis. The color map does not reach unity because of the downsampling effect.

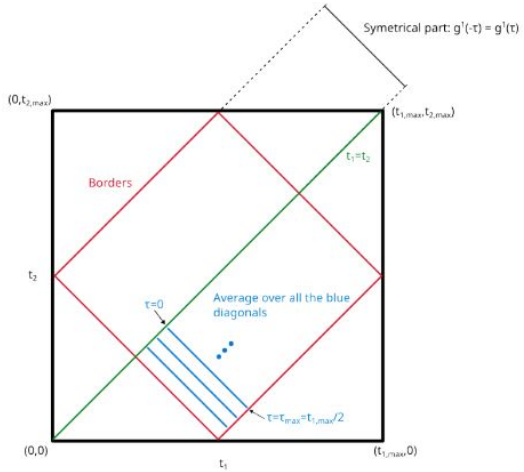

Figure 4.4: Diagram of the method to transform the map $|g^1(t_1, t_2)|$ to $|g^1(\tau)|$. The red box is the border of the summed data. The average is done along the blue diagonals and their symmetric along the green line where $t_1 = t_2$.

Stationary g¹ for a standard laser

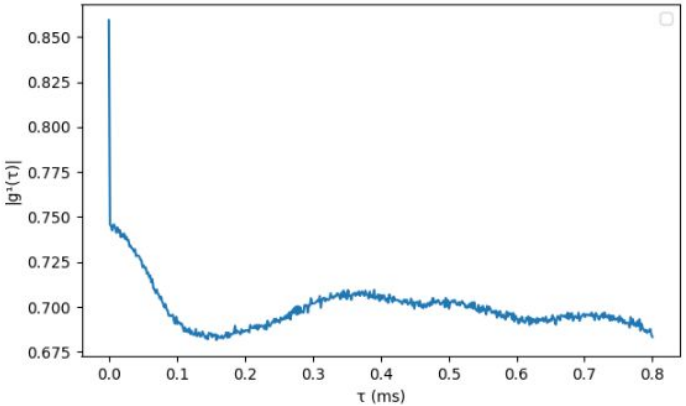

Figure 4.5: Approximation of $|g^1(\tau)|$ for the cavity laser. The curve does not reach unity for $\tau = 0$ because of the downsampling effect.

g^1 for the superradiant laser

Example of a collected signal (after a numerical band-pass filter applied)

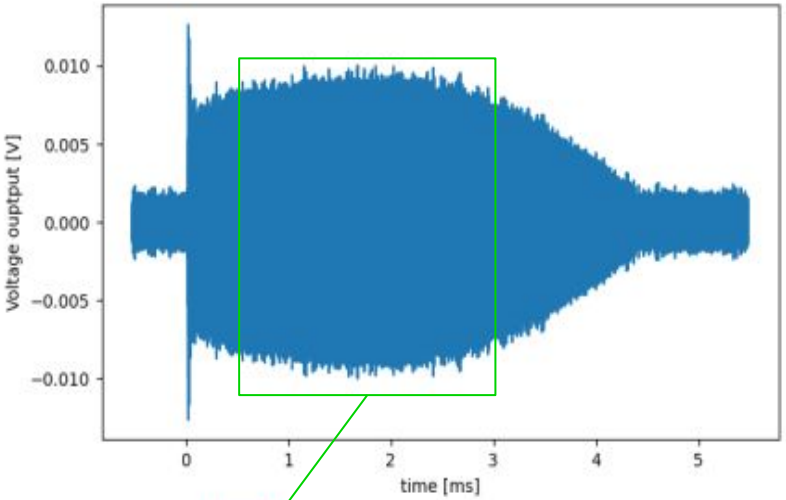

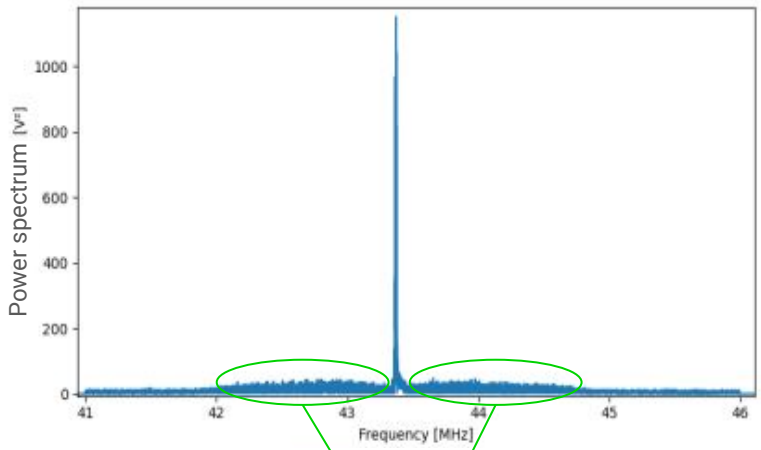

"Stationary" region with quasi-continous lasing

Additional features compared to the "standard" laser

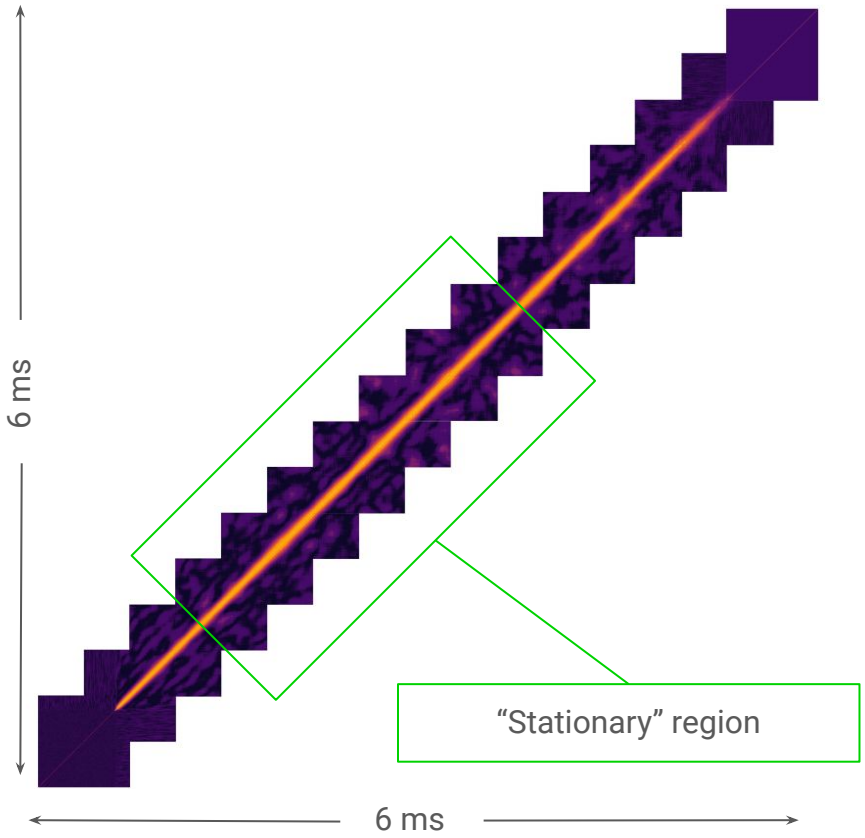

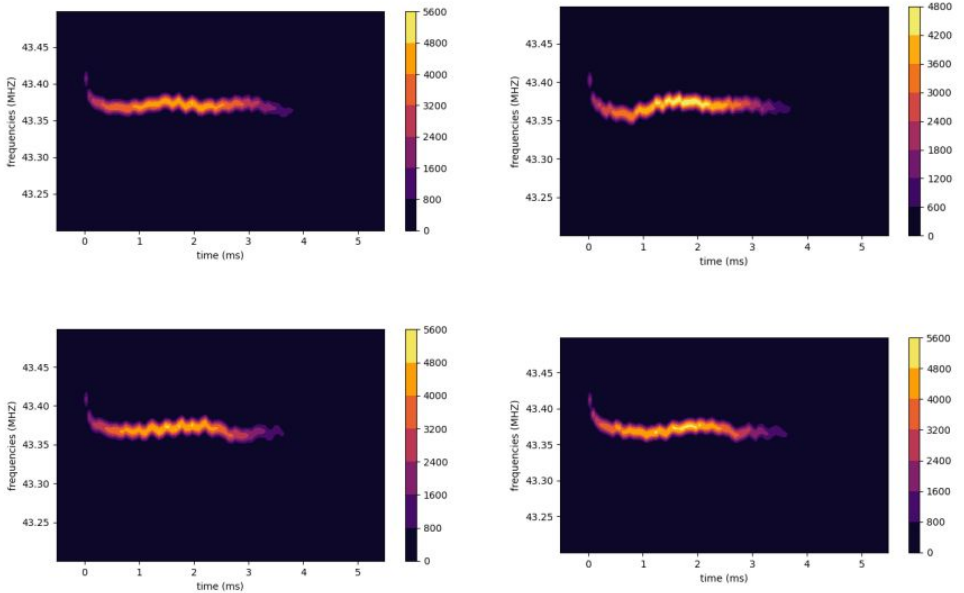

Figure 4.9: Spectrograms of four different recorded signals for the quasi-continuous superradiant laser. We can notice a common initial drift probably due to the time required for the laser to lock precisely to the cavity resonance.

Non-stationary g^1 for the superradiant laser

Stationary g¹ for the superradiant laser

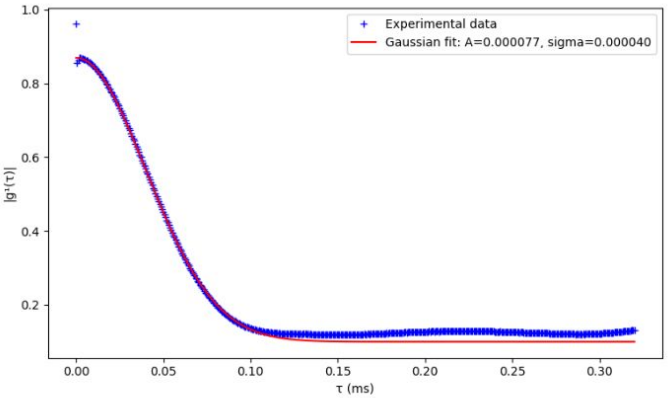

Figure 4.13: Approximation of $|g^1(\tau)|$ for the superradiant laser. The blue cross elements are the averaged samples whereas the red curve is a Gaussian fit. The first isolated blue point does not reach unity because of the downsampling effect. The Gaussian curves are lifted from the x-axis due to the finite amount of signal recorded (in theory, this plateau region after $\tau = 0.15$ ms should tend to zero).

Coherence time:

$$\tau_c \overset{\text{def}}{=} \int_{-\infty}^{+\infty} |g_1(\tau)|^2 \, d\tau \quad \Rightarrow \quad \tau_c \simeq 64 \ \mu\text{s}$$

Wiener-Khinchin theorem:

$$G^1(\tau) = \int_{-\infty}^{+\infty} S(\omega) e^{-i\omega\tau} \, d\omega \quad \Rightarrow \quad \text{FWHM} \simeq 2.355/\sigma \simeq 59 \ \text{kHz}$$

Numerical simulation as a comparison

Closed system interacting with a quantum bath

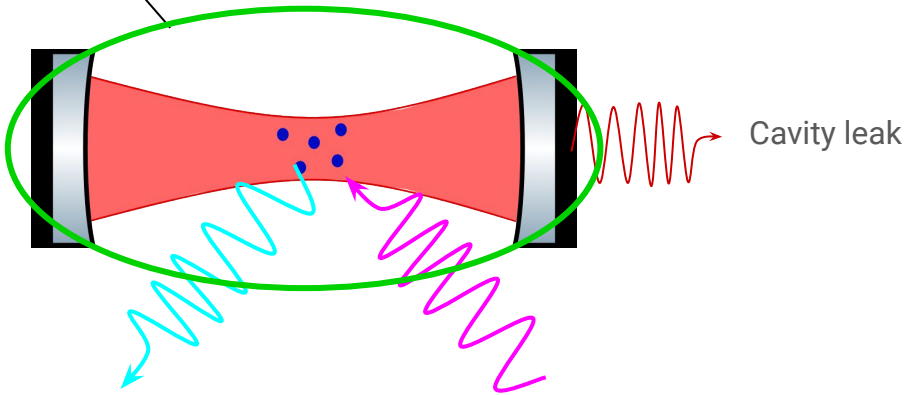

Type of exchange with the bath	Exchange rate	Associated operator
cavity leak	κ	$\hat{a}$
spontaneous decay into free space	γ	$\hat{S}_-$
repump	ν	$\hat{S}_+$
	γ_j	$\hat{L}_j$

Lindblad master equation: $$\dot{\hat{X}} = \frac{i}{\hbar}\left[\hat{H}, \hat{X}\right] + \sum_j \gamma_j \left(\hat{L}_j^\dagger \hat{X} \hat{L}_j - \frac{1}{2}\left\{\hat{L}_j^\dagger \hat{L}_j, \hat{X}\right\}\right)$$

Developing a set of differential equation and solving them lead to: $$g^1(\tau) = \frac{\left\langle \hat{a}^\dagger(\tau)\hat{a}(0)\right)\right\rangle}{\langle \hat{n} \rangle}$$

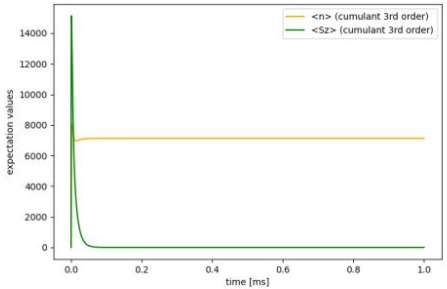

(a) Original plot with full time interval (0 to 1ms)

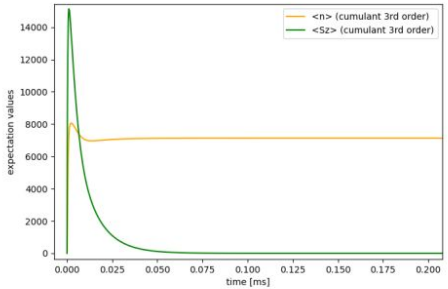

(b) Zoom on the main features (from 0 to 200 µs).

Figure 2.9: Simulation results for 100,000 atoms inside the cavity. Two types of expectation values are plotted: the photon number $\langle \hat{n} \rangle$ inside the cavity (green) and the atomic inversion $\left\langle \hat{S}_z \right\rangle$ (orange)

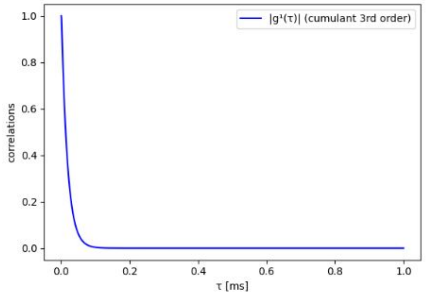

(a) Original plot with full time interval (0 to 1ms).

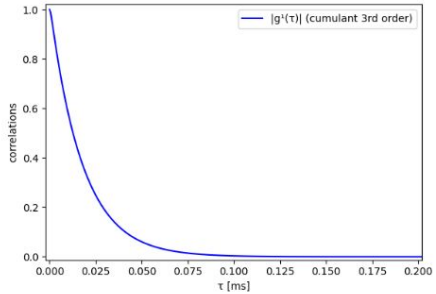

(b) Zoom on the main feature (from 0 to 200 µs).

Figure 2.11: Simulation results for 100,000 atoms inside the cavity. Plot of $|g^1(\tau)|$.

$$\tau_c \stackrel{\text{def}}{=} \int_{-\infty}^{+\infty} |g_1(\tau)|^2 \, d\tau \qquad \Rightarrow \qquad \tau_c \simeq 19 \text{ µs for } 100{,}000 \text{ atoms}$$

Conclusion

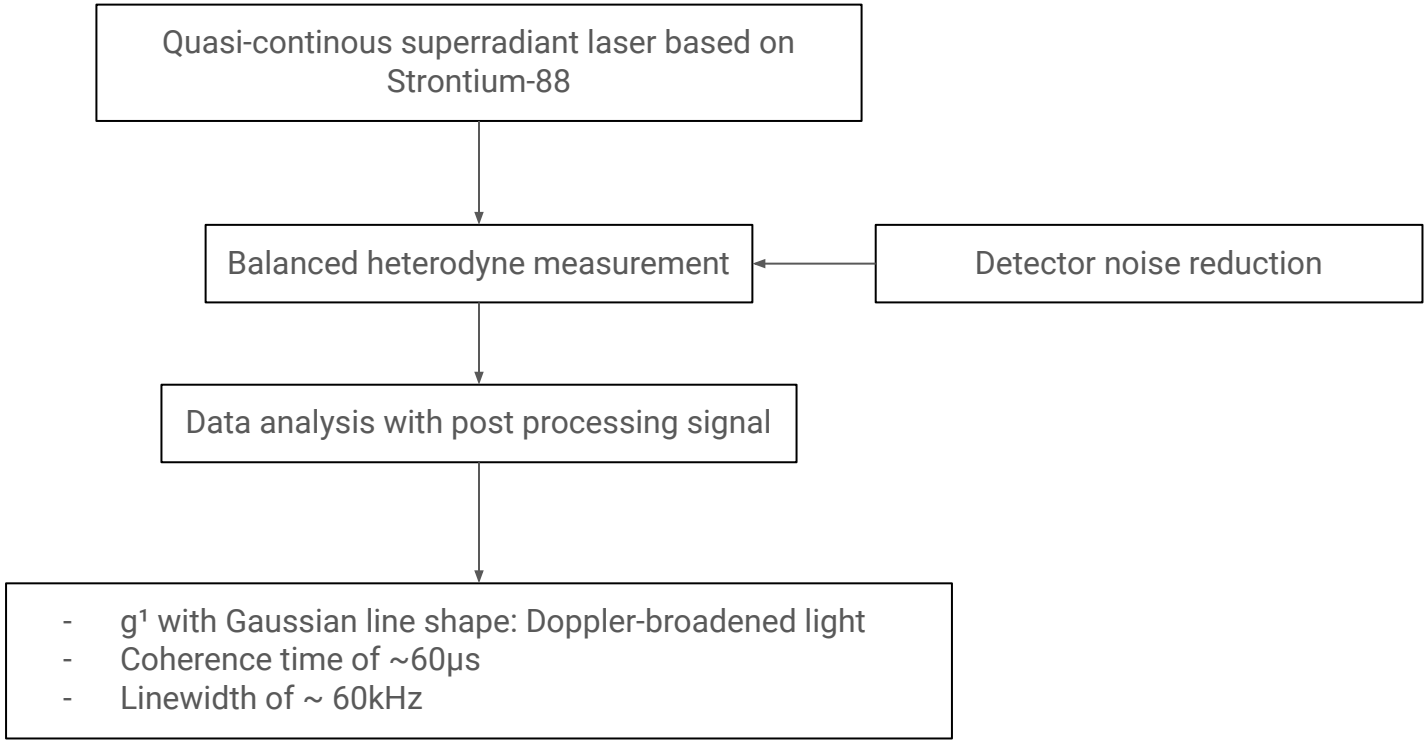
Quasi-continous superradiant laser based on Strontium-88
Balanced heterodyne measurement
Detector noise reduction
Data analysis with post processing signal
- g¹ with Gaussian line shape: Doppler-broadened light
- Coherence time of ~60μs
- Linewidth of ~ 60kHz

Thank you for your attention

Intensity calibration

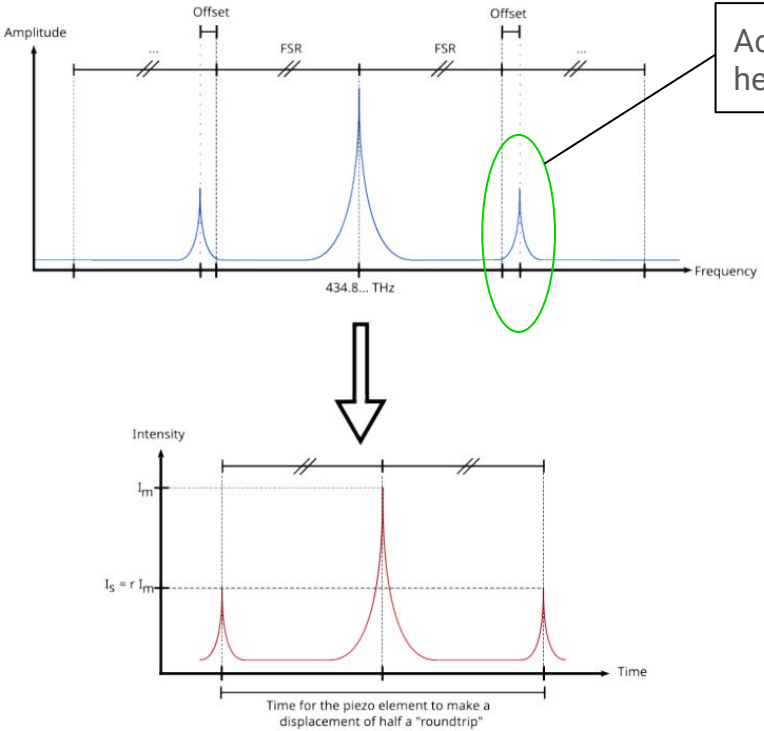

Figure 3.27: Spectrum of the fake laser with an offset on the sidebands giving three peaks for the intensity output. The intensity output varies between three different peaks as the piezo element contract or dilate: left sideband, carrier and right sideband frequencies are individually able to cross the cavity.

Actual sideband interacting with the local oscillator in the heterodyne experiment

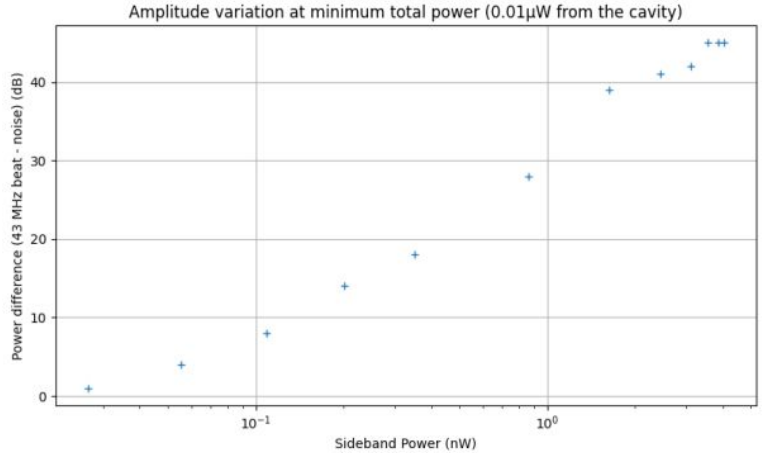

Figure 3.29: Beat power visibility on the oscilloscope (difference between the background noise and the top of the recorded beat) according to the light power of the associated sideband.